THE JOURNAL OF BIOLOGICAL CHEMISTRY
Vol. 274, No. 47, Issue of November 19, pp. 33235–33243, 1999

Printed in U.S.A.

The Cardiomyopathy and Lens Cataract Mutation in αB-crystallin Alters Its Protein Structure, Chaperone Activity, and Interaction with Intermediate Filaments *in Vitro**

(Received for publication, April 29, 1999, and in revised form, July 27, 1999)

Ming Der Perng‡§, Paul J. Muchowski§¶, Paul van den IJssel‡, Gabrielle J. S. Wu¶, Aileen M. Hutcheson‡, John I. Clark¶‖, and Roy A. Quinlan‡**

From the ‡Department of Biochemistry, Medical Science Institute, The University, Dundee DD1 5EH, United Kingdom and the Departments of ¶Biological Structure and ‖Ophthalmology, University of Washington, Seattle, Washington 98195-7420

Desmin-related myopathy and cataract are both caused by the R120G mutation in αB-crystallin. Desmin-related myopathy is one of several diseases characterized by the coaggregation of intermediate filaments with αB-crystallin, and it identifies intermediate filaments as important physiological substrates for αB-crystallin. Using recombinant human αB-crystallin, the effects of the disease-causing mutation R120G upon the structure and the chaperone activities of αB-crystallin are reported. The secondary, tertiary, and quaternary structural features of αB-crystallin are all altered by the mutation as deduced by near- and far-UV circular dichroism spectroscopy, size exclusion chromatography, and chymotryptic digestion assays. The R120G αB-crystallin is also less stable than wild type αB-crystallin to heat-induced denaturation. These structural changes coincide with a significant reduction in the *in vitro* chaperone activity of the mutant αB-crystallin protein, as assessed by temperature-induced protein aggregation assays. The mutation also significantly altered the interaction of αB-crystallin with intermediate filaments. It abolished the ability of αB-crystallin to prevent those filament-filament interactions required to induce gel formation while increasing αB-crystallin binding to assembled intermediate filaments. These activities are closely correlated to the observed disease pathologies characterized by filament aggregation accompanied by αB-crystallin binding. These studies provide important insight into the mechanism of αB-crystallin-induced aggregation of intermediate filaments that causes disease.

Desmin-related myopathy (DRM)[1] can be caused by mutations either in the intermediate filament protein desmin, or in the small heat shock protein αB-crystallin. Although several mutations in the intermediate filament protein desmin have been linked with DRM (1, 2), so far only a single mutation, R120G, in the small heat shock protein αB-crystallin has been identified (3). A characteristic disease pathology links the different causes of DRM, which consists of aggregates of intermediate filaments containing αB-crystallin present in the muscle cells of affected individuals (3, 4).

Other diseases, such as Alexander's disease (5) and drug-induced hepatitis (6), are also characterized by intermediate filament aggregates. These aggregates are typically co-associated with αB-crystallin (7) despite the fact that they involve different intermediate filament proteins. This suggests that the association of αB-crystallin with intermediate filament aggregates is independent of the specific intermediate filament protein but is rather a generic response to this pathological rearrangement of intermediate filaments. These data establish a clear link between αB-crystallin, intermediate filaments, and the disease-induced aggregation of intermediate filaments (8). The mechanism of intermediate filament aggregation and the role of small heat shock proteins in this process has yet to be addressed.

The recent assessment of sHSP activity *in vitro* has been based upon chaperone assays using either heat (9–11) or chemically unfolded substrates (12). These have been extremely useful for studying the role of ATP (13), post-translational modifications (11, 14–17), and specific αB-crystallin residues (18–22) in the chaperone activity of sHSPs. These studies mimic the role of sHSPs in stressed cells, but they do not identify the physiological targets or the role of sHSPs in unstressed cells.

The sHSPs are expressed in unstressed cells (8, 23–25) and sometimes at very high levels (26, 27). In unstressed, non-diseased cells of muscle (23), astrocyte (24, 25), and epithelial and lenticular origins (27), αB-crystallin is found associated with intermediate filaments. In the eye lens, there is a unique cytoskeletal filament that is a stable complex of α-crystallin, comprising both αB- and αA-crystallin, and lens intermediate filaments (28). This is called the beaded filament. Similar structures can be generated *in vitro* under appropriate coassembly conditions (29). These studies show that the association of sHSPs with intermediate filament networks is not just a stress-induced event (30), but is a feature of normal cells, and suggest a general role for sHSPs in intermediate filament biology.

Small HSPs bind to assembly competent intermediate filament proteins. This was demonstrated in the lens where a soluble complex of α-crystallin and intermediate filament proteins was immunopurified from lens cytosol (27, 31). It was subsequently demonstrated that sHSPs could inhibit GFAP as

* This work was supported by Wellcome Trust Grant No. 46747 (to R. A. Q. and P. v. d. I.), grants from the University of Dundee and the Overseas Research Student Award Scheme (to M. D. P.), and National Institutes of Health NEI Grant EY0452 (to J. I. C.) and NEI Vision Training Grant T32 EY07031 (to P. J. M.). The costs of publication of this article were defrayed in part by the payment of page charges. This article must therefore be hereby marked "*advertisement*" in accordance with 18 U.S.C. Section 1734 solely to indicate this fact.

§ These authors contributed equally.

** To whom correspondence should be addressed. Tel.: 44-1382-344752; Fax: 44-1382-201063; E-mail: raquinlan@bad.dundee.ac.uk.

[1] The abbreviations used are: DRM, desmin-related myopathy; BB, binding buffer; UVCD, ultraviolet circular dichroism; DTT, dithiothreitol; GFAP, glial fibrillary acidic protein; PMSF, phenylmethylsulfonyl fluoride; PAGE, polacrylamide gel electrophoresis; sHSP, small heat shock protein.

well as vimentin assembly *in vitro* (27). These data indicated that the association of sHSPs with intermediate filament proteins is not restricted to the filamentous form, but includes soluble intermediate filament complexes. From these observations, it is clear that sHSPs have the potential to influence intermediate filament assembly (29).

Recently, another aspect of the interaction of sHSPs with intermediate filaments was identified (32). Using a simple viscosity-based assay, sHSPs were shown to prevent gel formation by intermediate filaments, presumably by blocking non-covalent filament-filament interactions (32). These studies suggested a physiologically important link between intermediate filaments and sHSPs. In a cellular context, this link may prevent inappropriate interactions between bundled intermediate filaments (32). Abrogation of this sHSP function could lead to intermediate filament aggregate formation. This is not only relevant to DRM but also to other human diseases where this phenotype is a pathological hallmark such as Alexander's disease.

In this study, the structural and functional properties of the R120G αB-crystallin are compared with those of the wild type protein. Using several different *in vitro* assays, the effect of the mutation upon the chaperone activity of αB-crystallin has been studied. The UVCD, size exclusion chromatography and proteolysis studies all suggest that the mutation has affected the secondary, tertiary, and quaternary structure of αB-crystallin. The mutation also causes a significant reduction in the heat-induced denaturation and a reduction the *in vitro* chaperone activity of the protein. In order to understand how the αB-crystallin mutation could cause intermediate filament aggregation as seen in DRM, its effect upon the association with intermediate filaments was studied. The data show that R120G αB-crystallin was incapable of preventing filament-filament interactions that lead to the formation of an intermediate filament gel *in vitro*. This was accompanied by an apparent increase in the binding of R120G αB-crystallin to intermediate filaments. These data suggest that DRM resulting from the R120G mutation in αB-crystallin occurs as a progressive accumulation of intermediate filament aggregates brought about by the altered interaction of αB-crystallin with intermediate filaments.

MATERIALS AND METHODS

Expression Constructs for Recombinant αB-crystallins—Total RNA was isolated from a sample of human soleus muscle (RNeasy kit, Qiagen) and converted into cDNA (Life Technologies, Inc.; Superscript kit). Human αB-crystallin cDNA was amplified from this cDNA using oligonucleotides 5′-AGCCACCATGGACATCGC-3′ and 5′-CTATTTCTTGGGGGCTGCG-3′ as forward and reverse primer, respectively. The amplified product was cloned into the vector pGEM®-T Easy (Promega) and the sequence confirmed against the GenBank™ data base entry (accession no. S45630). The R120G mutation was introduced by two-step polymerase chain reaction using the pGEM-T Easy human αB-crystallin wild type vector as a template in the first amplification reaction. Overlapping, complementary oligonucleotides were constructed containing the desired A → G mutation at nucleotide position 358 as well as a silent A → G mutation at nucleotide position 363, 5′-TTCCACGGGAAGTACCGGATCCCAGC-3′ and 5′-CCGGTACTTCCCGTGGAACTCCCTGGAGATGAA-3′. Using all four oligonucleotides the mutated αB-crystallin cDNA was created in two consecutive amplifications, then subcloned. After verification of the sequences both the wild type and R120G αB-crystallin cDNAs were subcloned into the *Nde*I and *Eco*RI sites of the vector pET23b (Novagen).

Expression of Recombinant αB-Crystallins—Recombinant human αB-crystallins were expressed in BL21plysS(DE3) in the expression vector pET23b. Recombinant protein expression was induced using 0.5 mM isopropyl-1-thio-β-D-galactopyranoside for 4 h once the cultures had reached an OD_{600} of 0.6. Harvested bacterial pellets were resuspended in TEN buffer (50 mM Tris-HCl, pH 8, 1 mM EDTA, 300 mM NaCl, 0.2 mM PMSF, and 0.1% v/v of protease inhibitor mixture (Sigma)) and lysed by several freeze/thaw cycles. A supernatant fraction containing the soluble proteins including the recombinant sHSPs was prepared by centrifuging the lysate at 15,000 rpm in a JA20 rotor at 4 °C for 30 min. The supernatant was then dialyzed against column buffer.

Preparation of GFAP, Native, and Recombinant αB-crystallins—GFAP was purified from porcine spinal cord by axonal flotation as described previously (33). GFAP was then separated from the other neuronal intermediate filament proteins using DE52 (Whatman) in 8 M urea, 10 mM Tris-HCl, pH 8, 5 mM EDTA, and 25 mM 2-mercaptoethanol. The proteins were eluted with a 0–200 mM NaCl linear gradient. All column procedures were carried out at room temperature. Recombinant αB-crystallin was purified by both non-denaturing (34) and denaturing methods. In the latter, two diethylaminoethyl (DEAE) column steps were used. The supernatant fraction obtained from the bacteria was loaded onto the first column comprising TSK-DEAE 650M (Merck Ltd.) in 20 mM Tris-HCl, pH 8.0, 20 mM NaCl, 1 mM $MgCl_2$, 1 mM EDTA, 1 mM DTT, 0.2 mM PMSF and eluted with a 20–250 mM NaCl gradient. The sHSP-enriched fractions were pooled and dialyzed into buffer containing 6 M urea, 10 mM Tris-HCl, pH 8.0, 1 mM EDTA, 1 mM DTT, 0.2 mM PMSF. This was then loaded onto a DE52 column equilibrated in the same buffer. Proteins were eluted with a 0–200 mM NaCl gradient. All column steps were carried out at 4 °C. Column fractions were checked for homogeneity by SDS-PAGE. Protein concentrations were determined by the Bradford protein assay.

Analytical Size Exclusion Chromatography—Analytical size-exclusion chromatography was performed on a Biosep-SEC-S4000, 7-μm, 300 × 7.8-mm column using a Hewlett-Packard high performance liquid chromatograph with the following mobile phase: 0.1 M potassium phosphate, pH 7.0 and 0.2 M NaCl, at a flow rate of 0.5 ml/min. High molecular weight protein standards (Amersham Pharmacia Biotech) were used to calibrate the column. The standard deviation of the molecular masses of wild type αB-crystallin/αB-crystallin mutants was determined from the peak width at its half-height in six independent experiments.

Proteolytic, Spectroscopic, and in Vitro Chaperone Analyses—Proteolysis of wild type αB-crystallin/αB-crystallin mutants was performed as described previously (22, 35). CD spectra were measured as described previously (36, 37). The presented CD spectra are the average of 16 scans, smoothed by polynomial curve fitting. The fit was checked with a statistical test so that the original data was not over-smoothed. To calculate molar ellipticity, a residue molecular weight of 115 was assumed. The proteins were dissolved in 20 mM sodium phosphate (pH7.1) and used at concentrations of 0.5 and 1.0 mg/ml for far- and near-UVCD, respectively, as determined from calculated extinction coefficients based on a protein amino acid sequence as described previously (38, 39). The pathlength of the cells was 10 mm for near-UVCD and 1.0 mm for far-UVCD spectroscopy.

Temperature-dependent precipitation of wild type and R120G αB-crystallin was measured in a Beckman DU640 spectrophotometer equipped with a Peltier temperature controlled cuvette holder. The rate of temperature increase was 0.1 °C/min. Proteins were dialyzed into 20 mM sodium phosphate, pH 7.1, and the concentration adjusted to 0.5 mg/ml prior to the assay. First derivative calculation was used to determine the temperature at which 50% precipitation had occurred.

Temperature-induced aggregation assays using citrate synthase (10) and alcohol dehydrogenase (11) as target proteins were performed as described (13, 40).

Intermediate Filament Assembly, Binding, and Viscosity Assays Involving αB-crystallin—The sedimentation assay as developed by Nicholl and Quinlan (27) was used to assess the ability of sHSPs to inhibit intermediate filament assembly. Purified porcine GFAP was used for these studies. αB-crystallins were added to GFAP in 8 M urea, 20 mM Tris-HCl, pH 8.0, 5 mM EDTA, 25 mM 2-mercaptoethanol prior to the assembly assay. The final dialysis was against assembly buffer: 10 mM Tris-HCl, pH 7.0, 25 mM 2-mercaptoethanol, 50 mM NaCl. The experiments were performed at room temperature. Dialysates were layered onto a 0.85 M sucrose cushion in the assembly buffer and centrifuged at 80,000 × *g* for 30 min at 20 °C in a Beckman TLA-55 rotor using a TL100 benchtop ultracentrifuge. The pellet and supernatant fractions were compared by SDS-PAGE as described previously (27).

For the intermediate filament binding assay, αB-crystallins were again mixed with GFAP in 8 M urea, 20 mM Tris-HCl, pH 8.0, 5 mM EDTA, 25 mM 2-mercaptoethanol and then stepwise dialyzed into 10 mM Tris-HCl, pH 8.0, 25 mM 2-mercaptoethanol. Assembly of the GFAP intermediate filaments and binding of the αB-crystallins was then induced by addition of a 20-fold concentrated binding buffer (BB) to give a final concentration of 100 mM imidazole-HCl, pH 6.8, 0.5 mM DTT and incubation at the indicated temperature.

The gel formation assay was based upon a method used to monitor

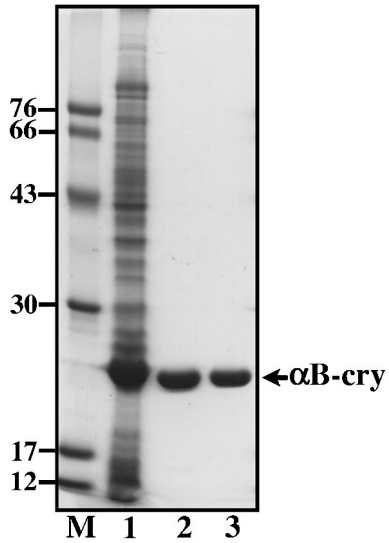

FIG. 1. **SDS-PAGE analysis of purified wild type αB-crystallin and mutant R120G αB-crystallin.** A 12% w/v gel was used as the separating gel and proteins were visualized using the dye, Coomassie Blue R250. Molecular size standards (*lane M*; $M_r \times 10^{-3}$) are shown and labeled adjacent to *lane 1*. *Lane 1*, overexpression of wild type αB-crystallin in *E. coli*; *lane 2*, 1 μg of purified wild type αB-crystallin; *lane 3*, 1 μg of R120G αB-crystallin. Position of the αB-crystallin is indicated by an *arrow*.

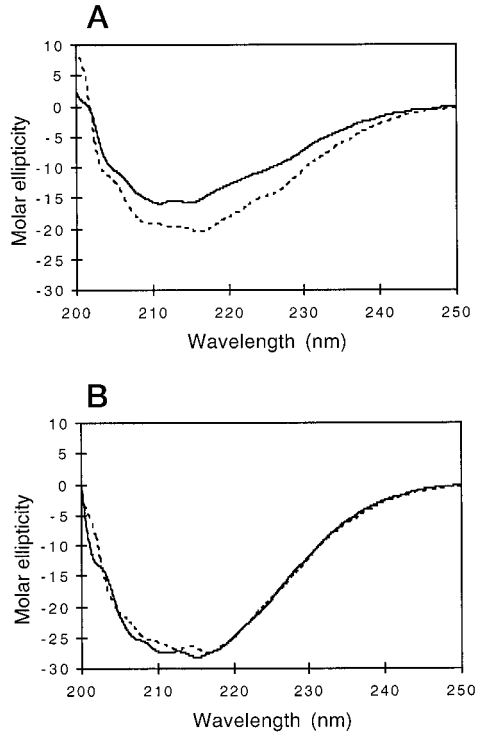

FIG. 2. **Far-UV CD spectra of wild type αB-crystallin and mutant R120G αB-crystallin at 25 and 45 °C.** The spectra at 25 (——) and 45 °C (- - -) for wild type αB-crystallin (*A*) and R120G αB-crystallin (*B*) are shown and represent an average of 16 scans, smoothed by polynomial curve fitting. The protein concentrations were 0.5 mg/ml, and the pathlength of the cell was 1.0 mm. The CD molar ellipticity units are degrees cm^2/dmol.

actin binding protein activity by falling ball viscometry (41). Filament assembly was promoted exactly as described for the binding assay by addition of the 20-fold concentrated BB. 100 μl of sample was loaded into a glass tube to be used in the viscosity assay. This was then immersed in a 37 °C water bath for 1 h prior to conducting the gel formation assay. A ball was then placed into the tube, and the ability of the solution to support the ball was monitored.

Electron Microscopy—Protein samples were diluted to 100–200 μg/ml, and negatively stained using 1% w/v uranyl acetate. Grids were examined in a Jeol 1200EX TEM, using an accelerating voltage of 80 kV.

RESULTS

Structure and Stability Characteristics of the R120G αB-crystallin Compared with Wild Type—The effect of the disease causing mutation R120G on the structure of αB-crystallin was examined using near- and far-UVCD spectroscopy. The wild type and mutant αB-crystallin were expressed in *Escherichia coli* using a pET-based vector system and purified to homogeneity by ion exchange chromatography. The sample purity was assessed by SDS-PAGE and is presented in Fig. 1.

Using recombinantly produced proteins, the far-UVCD spectrum (200–250 nm) was measured for both wild type and mutant αB-crystallin (Fig. 2, *A* and *B*). At 25 °C (Fig. 2*A*), the far-UVCD spectrum of wild type αB-crystallin contained a peak minimum at approximately 215 nm that is consistent with previous UVCD analyses showing a high percentage of β-sheet/β-turn structure in αB-crystallin (34, 37, 42). When tested under identical conditions, the R120G mutant displayed a peak minimum that was shifted to a slightly shorter wavelength and had a significant (44%) increase in negative molar ellipticity in comparison to wild type αB-crystallin at 220 nm (Fig. 2*A*). A second measurement was made for both proteins at 45 °C to assess protein stability at temperatures utilized in the chaperone assays (Fig. 2*B*). While the magnitude of the peak minimum (215 nm) for wild type αB-crystallin increased approximately 22% at 45 °C, there was no increase for the R120G mutant (Fig. 2*B*).

At 25 °C, the near UVCD spectrum of wild type αB-crystallin included four positive ellipticity peaks below 290 nm and a large negative peak at approximately 295 nm (Fig. 3*A*), consistent with past studies using αB-crystallin (34, 37, 42). In stark contrast, peaks below 290 nm in the near-UVCD of the R120G mutant were shifted significantly toward negative ellipticity values at 25 °C and only a small negative peak was observed at 295 nm (Fig. 3*A*). For wild type αB-crystallin, increasing the temperature from 25 to 45 °C resulted in a large shift in ellipticity from positive to negative values below 290 nm, but had essentially no effect on the ellipticity of the 295 nm peak (Fig. 3*B*). For the R120G mutant, an increase from 25 to 45 °C resulted in only a modest shift toward negative ellipticity values below 290 nm, and did not significantly affect the ellipticity at 295 nm (Fig. 3*B*). Both the far- and near-UVCD data indicate that the R120G mutation has altered the secondary and tertiary structure of the αB-crystallin.

The quaternary structure of R120G αB-crystallin was altered, as assessed by six independent size exclusion chromatography analyses. The protein complexes formed by the R120G αB-crystallin mutant were larger (M_r = 823,000 ± 131,000) compared with the wild type (M_r = 633,000 ± 80,000) and more disperse, as seen by the broader size distribution given by the standard deviations.

Since the structure of αB-crystallin was affected by the R120G mutation, we decided to assess its temperature stability. Protein aggregation was detected by light scattering (Fig. 4) and showed that both wild type and R120G αB-crystallin did not aggregate up to 55 °C. Above this temperature, the mutated protein started to aggregate with precipitation 50% complete at 57.2 °C, whereas the wild type αB-crystallin remained soluble up to 63 °C, showing 50% precipitation at 64.5 °C. Furthermore, the aggregation of the R120G αB-crystallin occurred over a wider temperature range than that of the wild type protein (Fig. 4). Thus, the mutation does appear to affect the stability of the protein, but only at higher (>55 °C), non-phys-

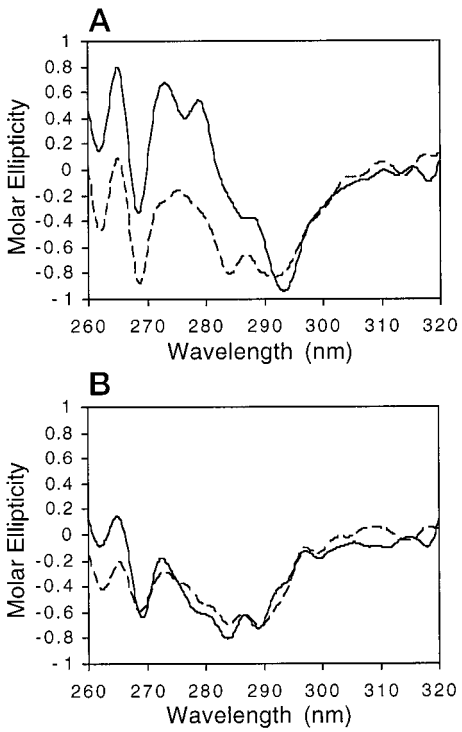

FIG. 3. **Near-UV circular dichroism spectra of wild type αB-crystallin and mutant R120G αB-crystallin at 25 and 45 °C.** The spectra for wild type αB-crystallin (*A*) and R120G αB-crystallin (*B*) are shown and represent an average of 16 scans, smoothed by polynomial curve fitting. The protein concentrations were 1.0 mg/ml, and the pathlength of the cell was 10.0 mm. The CD molar ellipticity units are degrees cm^2/dmol. Spectra for both αB-crystallins were obtained at 25 (——) and 45 °C (- - -).

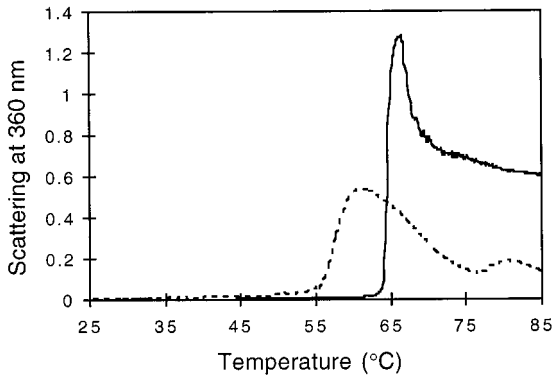

FIG. 4. **Temperature stability of wild type and R120G αB-crystallin.** Aggregation of wild type (——) and R120G (- - -) αB-crystallin was assessed as a function of temperature from 25 to 85 °C by light scattering at 360 nm. Protein concentration was 0.5 mg/ml in 20 mM sodium phosphate, pH 7.1. The temperature was increased by 0.1 °C/min. Temperatures at midpoint of precipitation were calculated to be 64.5 and 57.2 °C for wild type and R120G αB-crystallin, respectively. Note the different slopes of precipitation for the wild type and the mutant proteins.

iological temperatures.

To assess whether the R120G mutation affected the stability of αB-crystallin below 55 °C, the temperature dependence of the ellipticity at 205 and 217 nm was studied by far-UVCD (data not shown). A gradual conformational transition was shown between 25 °C and 55 °C for the wild type, but not the mutated αB-crystallin. This is consistent with the far-UVCD spectra (Fig. 2, *A* and *B*, *cf.* spectra at 25 °C *versus* 45 °C) and indicates that the stability of the mutated protein was not affected below 55 °C.

The Effect of the R120G Mutation upon the Chymotryptic

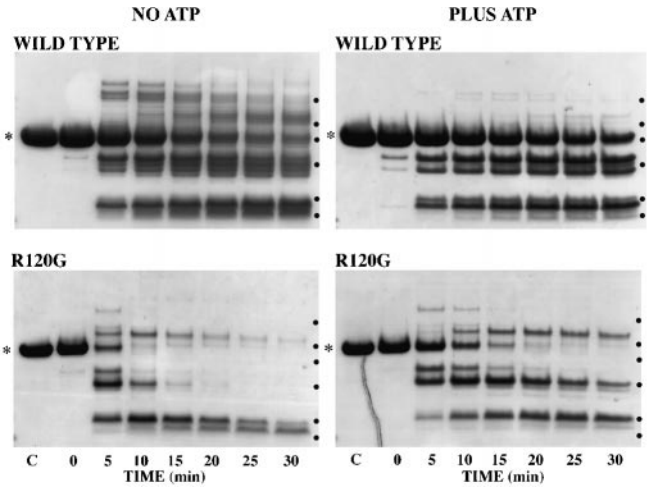

FIG. 5. **SDS-PAGE analysis of the chymotryptic digestion of wild type αB-crystallin and R120G αB-crystallin in the absence (*NO ATP*) and presence of ATP (*PLUS ATP*) at 37 °C.** Samples were taken over a 30-min time course. In the absence of ATP, the pattern of proteolysis for R120G αB-crystallin was similar but not identical to the pattern observed for wild type αB-crystallin. Substantial increase in the susceptibility to proteolysis was noted for R120G αB-crystallin. The pattern of proteolysis obtained for R120G αB-crystallin in the presence of ATP resembled that of wild type αB-crystallin, although again the mutant was more susceptible than the wild type protein. These data suggest that the mutation certainly changed accessibility to the chymotryptic cleavage sites in αB-crystallin. Undigested protein is indicated (*). Molecular size markers are indicated (●) and correspond to 36.5, 31, 21.5 14.4, 6 and 3.5 kDa.

Digestion of αB-crystallin—Chymotrypsin has been used to assess the susceptibility of αB-crystallin to proteolysis (22, 35). ATP has been shown to increase the protection of some of these sites in the α-crystallin domain against chymotryptic digestion (22, 35). These assays were used to evaluate the effects of the R120G mutation upon the availability of the chymotryptic sites for digestion as another indicator of changes in the structural characteristics of αB-crystallin (Fig. 5). The R120G mutation did make the chymotryptic sites more accessible compared with the wild type (Fig. 5), as the R120G mutant was digested faster than wild type αB-crystallin. The pattern of proteolytic products produced was qualitatively similar but not the same. Protection of the chymotrypsin sites was afforded upon addition of ATP to both the R120G and wild type αB-crystallin (Fig. 5). Thus, at this level, the differences in the digestion characteristics of R120G αB-crystallin suggested that there had indeed been some structural changes as a result of the mutation, but these did not appear to significantly alter the region(s) of αB-crystallin involved in interacting with ATP.

In Vitro Chaperone Assays—Prior to the discovery of the physiological substrates for αB-crystallin, *in vitro* assays were developed based upon heat-induced aggregation of proteins to assess the chaperone activity of αB-crystallin. Two were selected to cover a range of chaperone: substrate concentrations and also a range of temperatures (10, 11). As shown in Table I, R120G αB-crystallin was worse than the wild type αB-crystallin in both chaperone assays. The R120G mutant was also tested at molar ratios of 2:1 and 10:1 (protein:αB-crystallin) using citrate synthase as the assay substrate and gave similar results to those obtained at a 1:1 ratio (Table I). In addition, at both 10:1 and 5:1 (protein:αB-crystallin) in the alcohol dehydrogenase-based chaperone assay, similar results to the 20:1 ratio were obtained (Table I). Therefore, it is reasonable to expect that the mutation will compromise the ability of αB-crystallin to perform its chaperone role in muscle and lens cells.

Intermediate Filament Assembly, Binding, and Gel Forming Assays—As demonstrated by the discovery of the disease caus-

TABLE I
The chaperone activities of αB-crystallin and R120G αB-crystallin compared using the alcohol dehydrogenase and citrate synthase assays

The R120G αB-crystallin was worse in all instances than the wild type αB-crystallin.

Protein assay	% Protein aggregation	
	Wild type αB-crystallin	R120G αB-crystallin
Alcohol dehydrogenase (ADH): protein ratio = 20:1 (ADH:αB); assay temperature = 37 °C	29 ± 2	90 ± 7
Citrate synthase: protein ratio = 1:1; assay temperature = 45 °C	9 ± 1	37 ± 6

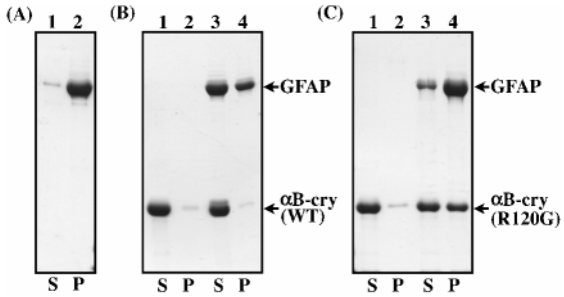

FIG. 6. **Effect of wild type and R120G αB-crystallin on GFAP assembly *in vitro*.** In the assembly inhibition assay, GFAP was assembled *in vitro* (*A*) in the presence of wild type αB-crystallin (*B*) and R120G αB-crystallin (*C*) in a molar ratio of 1:2 at 22 °C. The supernatant (*S*) and pellet fractions (*P*) were analyzed by SDS-PAGE and stained with Coomassie R250. The positions of GFAP and αB-crystallin are indicated (*B* and *C*). Under these conditions of assembly, most of the GFAP is sedimented (*A*, *lane 2*), with only a small proportion of the protein remaining in the supernatant (*A*, *lane 1*). Contrast this result to the assembly of GFAP in the presence of αB-crystallin (*B*), where >50% of the GFAP remains in the supernatant (*B*, *lane 3*). Notice that using these assay conditions, nearly all the wild type αB-crystallin remained in the supernatant fractions in the absence (*B*, *lane 1*) and presence of GFAP (*B*, *lane 3*). In the presence of R120G αB-crystallin (*C*), >80% of the GFAP is found in the pellet (*P*; *C*, *lane 4*). In the presence of R120G αB-crystallin, the soluble GFAP remaining in the supernatant (*C*, *lane 3*) is reduced compared with the coassembly of GFAP with wild type αB-crystallin (*B*, *lane 3*) but greater than the control assembly for GFAP (*A*, *lane 1*). Notice too that the R120G αB-crystallin bound to the filaments in the pellet fraction (*C*, *lane 4*) in complete contrast to wild type αB-crystallin (*B*, *lane 4*) under similar experimental conditions. In the absence of GFAP filaments, most R120G αB-crystallin remained soluble (*C*, *lane 1*) with only a very small proportion sedimenting under these conditions (*C*, *lane 2*).

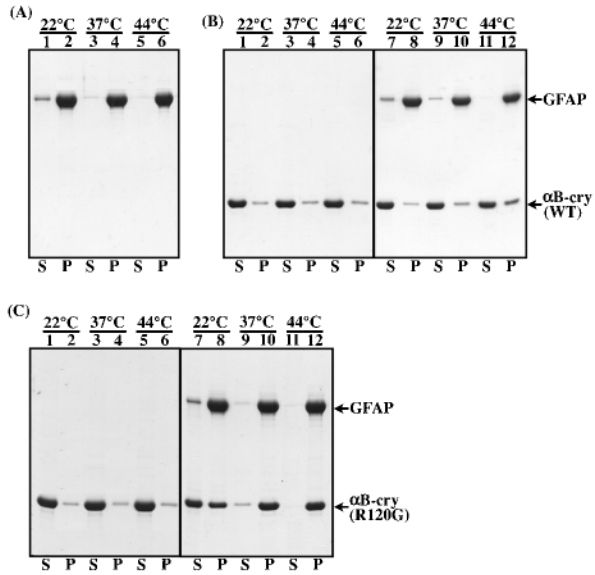

FIG. 7. **Binding of wild type and R120G αB-crystallin to GFAP filaments *in vitro*.** In this assay, the GFAP assembly was conducted under conditions that promoted αB-crystallin binding to intermediate filaments (32). The binding is a temperature-dependent process (30, 32), and the three temperatures selected are indicated above the relevant gel lanes (*A–C*). The pellet (*P*) and supernatant (*S*) fractions were analyzed by SDS-PAGE and stained with Coomassie Blue R250. GFAP assembled efficiently into filaments under these assay conditions at temperatures of 22, 37, and 44 °C (*A*). Most of the GFAP is present in the pellet fractions (*A*, *lanes 2*, *4*, and *6*, labeled *P*). The small proportion of GFAP remaining in the supernatant (*A*, *lanes 1*, *3*, and *5*, respectively, labeled *S*) varies with temperature. In the absence of GFAP, wild type (*B*, *lanes 1*, *3*, and *5*) and R120G αB-crystallin (*C*, *lanes 1*, *3* and *5*) remained almost entirely soluble (labeled *S*). When GFAP is included in the assay, both wild type αB-crystallin (*B*, *cf. lanes 8*, *10*, and *12*) and R120G αB-crystallin (*C*, *cf. lanes 8*, *10*, and *12*) sedimented with the GFAP filaments. This was temperature-dependent, as an increasing proportion of wild type αB-crystallin and R120G αB-crystallin was found in the pellet fractions (*B* and *C*, *lanes 8*, *10*, and *12*). Note that in the presence of GFAP, an appreciable proportion of the R120G αB-crystallin was pelletable even at 22 °C (*C*, *lane 8*). At 44 °C, all the R120G αB-crystallin was present in the pellet fraction (*C*, *lane 10*). The wild type αB-crystallin was found in the pellet fractions at 37 °C (*B*, *lane 10*) and 44 °C (*B*, *lane 12*), but larger proportion remained in the soluble fractions at both temperatures (*B*, *lanes 9* and *11*, *cf. lanes 11* and *12*).

TABLE II
Summary of the data collected for the effect of αB-crystallin and the R120G mutant on gel formation by intermediate filaments as monitored by a falling ball viscometry assay

GFAP can form a protein gel capable of supporting a small ball bearing. Including αB-crystallin in with GFAP prevented gel formation and allowed the ball to drop to the bottom of the tube. The R120G mutation abrogated this activity of αB-crystallin.

Chaperone added to assay	GFAP gel formation as indicated by the ball position in the viscometer
No addition	Top
αB-crystallin	Bottom
R120G αB-crystallin	Top

ing mutation in αB-crystallin, intermediate filaments are a physiological target of αB-crystallin. Three assays had been developed that assess the interaction of αB-crystallin with intermediate filament proteins at different levels (32). These are the ability of αB-crystallin to (*a*) inhibit filament assembly, (*b*) bind to and co-sediment with intermediate filaments, and (*c*) prevent filament-filament interactions as measured by falling ball viscometry (32). The effect of the mutation R120G upon αB-crystallin chaperone activity was tested using these assays. The intermediate filament protein, GFAP, was used. GFAP is a physiologically relevant target because of the formation of Rosenthal fibers, which contain GFAP filaments coaggregated with αB-crystallin in the neurodegenerative disease Alexander's disease (5). It is also a type III intermediate filament protein closely related to desmin (43) with similar structural features and mechanisms of assembly.

In Figs. 6 and 7, the effect upon intermediate filament assembly (Fig. 6) and the ability to bind to intermediate filaments (Fig. 7) was examined. These assays are conducted at different pH and salt conditions to optimize for the inhibition of assembly and binding to intermediate filaments, respectively (30, 32). As can be seen in Fig. 6, R120G αB-crystallin was reduced in its ability to inhibit the assembly of the intermediate filament protein, GFAP. Compared with the assembly of GFAP in the

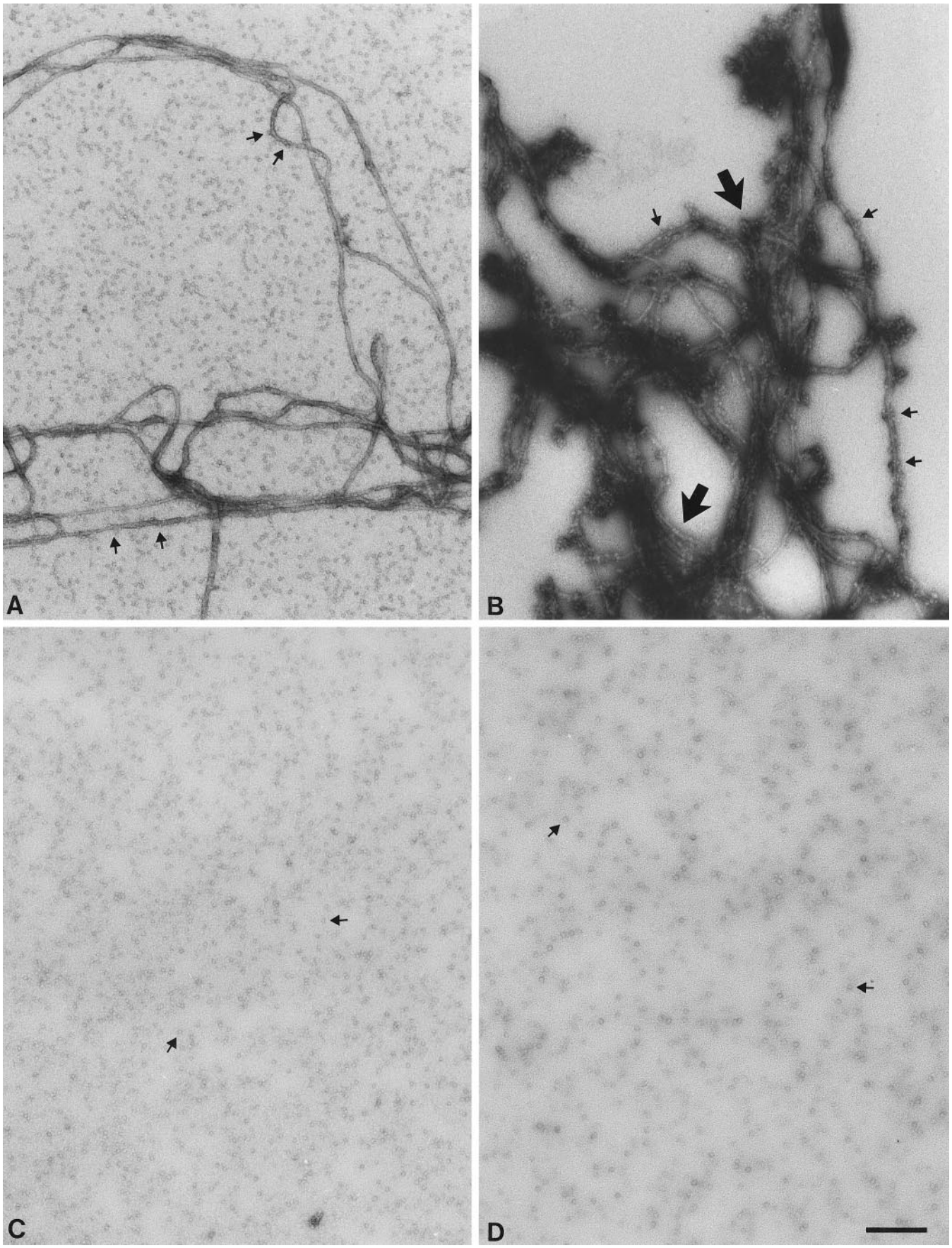

FIG. 8. **Visualization of intermediate filaments assembled in the presence of wild type and R120G αB-crystallin.** Samples were taken at the completion of the viscosity assay and processed using the negative staining technique for electron microscopy. In the presence of wild type αB-crystallin (*A*), the intermediate filaments formed were long and sometimes had αB-crystallin particles attached (*arrows*). The filaments were generally not clumped in this preparation. In contrast, filaments co-assembled in the presence of R120G αB-crystallin (*B*) were clumped (*large*

absence of αB-crystallin (Fig. 6, *lanes 1* and *2*), the R120G αB-crystallin was still able to partially inhibit GFAP assembly (Fig. 6, *lanes 3* and *4*). Moreover, a sizeable proportion of R120G αB-crystallin was found in the pellet fraction (Fig. 6*C*, *lane 4*), even at 22 °C, the temperature of this assay. The wild type αB-crystallin remained almost completely soluble under these conditions (Fig. 6*B*, *lane 4*). This was the first indication that R120G αB-crystallin bound more avidly to intermediate filaments than the wild type protein.

The increased binding of R120G αB-crystallin (Fig. 7*C*) to GFAP filaments compared with the wild type protein (Fig. 7*B*) was a dramatic effect of the mutation. Even at 37 °C, R120G αB-crystallin was found to bind almost completely to the pelletable GFAP filaments, whereas the wild type αB-crystallin was only partially bound (<20%). This increased binding was consistent at different molar ratios, from 1:2 to 2:1 (sHSP to GFAP, respectively) and was apparently unaffected by the presence of 1 mM ATP (data not shown).

The increased binding of R120G αB-crystallin to intermediate filaments might be expected to increase its ability to prevent filament-filament interactions either indirectly by steric hindrance or directly by obscuring the filament-filament interaction sites. Using falling ball viscometry, this hypothesis was tested. The assay was developed so that GFAP forms a protein gel in the tube in the absence of αB-crystallin. The buffer conditions are the same as those used for the filament binding assay. This gel is capable of supporting the ball used in the viscosity assay. Addition of αB-crystallin prevents gel formation and so permits the ball to sink to the bottom of the tube (32). This is the result of inhibiting non-covalent filament-filament interactions rather than preventing filament formation as these assay conditions were similar to those used in the filament binding assay (Fig. 7), where no loss of sedimentable GFAP was observed (see also Ref. 32). As expected, after assembly of GFAP in the absence of sHSP in the control tube, a gel formed preventing the ball from falling. The presence of wild type αB-crystallin in the assay mixture at a 2:1 molar ratio to GFAP prevented the filaments formed from supporting the ball in the viscometer. In contrast, the mutant R120G αB-crystallin appeared completely ineffective at inhibiting gel formation and thus the ball was unable to enter the viscometer. Similar results were obtained for the ratios 1:2 and 2:1, sHSP to GFAP, respectively, and in the presence of 1 mM ATP (data not shown). Table II summarizes data obtained from three separate experiments.

The data from the viscosity assays have demonstrated that the R120G mutation abolished the ability of αB-crystallin to prevent gel formation by failing to inhibit filament-filament interactions required in this process, despite the increased ability of the mutant R120G αB-crystallin to bind to intermediate filaments (Fig. 7).

Visualization of the αB-crystallin Intermediate Filament Complex by Electron Microscopy—To examine the association of αB-crystallin with the GFAP filaments during the binding/viscosity assays, samples were examined using negative staining techniques and electron microscopy (Fig. 8). At 37 °C, limited binding of wild type αB-crystallin to GFAP filament was observed (Fig. 8*A*, *arrows*), whereas the R120G αB-crystallin particles were very closely associated with filaments (Fig. 8*B*, *arrows*) with no particles left unbound. In the absence of GFAP filaments, both wild type (Fig. 8*C*) and R120G αB-crystallin (Fig. 8*D*) formed discrete particles approximately 15–20 nm in diameter (Fig. 8, *C* and *D, arrows*). These observations correlated with the binding assay results (Fig. 7, *B* and *C*), where almost all of the mutant αB-crystallin bound the GFAP filaments compared with a much smaller proportion of the wild type protein. From the electron micrographs, it appears that the increased binding of the mutant αB-crystallin resulted in a very extensive coating of the intermediate filaments, leading to filament bundling (Fig. 8*B*).

DISCUSSION

The R120G mutation in αB-crystallin affects a highly conserved residue among the whole sHSP family (44, 45). It is important for the function of αA- and αB-crystallin as mutating this residue causes the human diseases, cataract (46) and DRM (3), respectively. Other mutational studies using the *Mycobacterium tuberculosis* sHSP, HSP16.3, and the mammalian sHSPs HSP27 and αA-crystallin (21) also show this highly conserved arginine residue is structurally very important as it is part of a β-strand involved in subunit interactions (21). Recently, the crystal structure of the *Methanococcus jannaschii* sHSP, HSP16.5, has been described (47), and this provided the first atomic details of this conserved arginine residue. From these data, a direct or indirect role for the disease causing arginine residue in subunit-subunit interactions was proposed (48). Although a recent study reported on the structural and chaperone-like properties of R120G αB-crystallin (49), we initiated our studies to investigate the interaction with intermediate filaments, the physiologically relevant target of αB-crystallin given the fact the mutation causes intermediate filament aggregation in the disease DRM (3).

Secondary, Tertiary, and Quaternary Structure of αB-crystallin Is Altered by the Mutation R120G—The far- and near-UVCD data presented here for the recombinant αB-crystallin (Figs. 2 and 3) correlate well with previously published data (22, 34, 37, 42). Increasing the temperature from 25 to 45 °C resulted in shifts in ellipticity values in the far- (50) and near-UV (50, 51) for wild type αB-crystallin that are consistent with a conformational change. The far- and near-UVCD spectra obtained for the R120G αB-crystallin demonstrated that the mutation affected the secondary and tertiary structure of the protein. Interestingly, the UVCD spectrum of R120G αB-crystallin at 25 °C appeared similar to that obtained for the wild type αB-crystallin at 45 °C, suggesting that the R120G αB-crystallin already existed in a more open, even partially unfolded, conformation at 25 °C. In the closely related protein, αA-crystallin, mutation of the equivalent arginine residue (Arg-116) to a cysteine and subsequent spin label modification also changed the secondary, tertiary and quaternary structure of the protein (52). The R120G mutation in αB-crystallin modified the protein structure such that the accessibility of the chymotryptic sites was increased (Fig. 5).

Changes in the quaternary structure were therefore expected and this is substantiated by the results obtained from size exclusion chromatography. The R120G mutation induced an increase in the average M_r and a broadening of the M_r range of αB-crystallin. A similar effect upon the M_r and therefore the quaternary structure of αA-crystallin was also observed (21, 52) when the equivalent arginine (Arg-116) was changed. In the case of HSP27, oligomerization of the α-crystallin domain (21) was affected by mutating the equivalent arginine (Arg-140), but here the M_r decreased. Obviously, while it can be concluded that this conserved arginine performs a key structural role, the effect of changing this residue is not necessarily the same for all the different sHSPs.

arrows). Co-aggregation between intermediate filaments and R120G αB-crystallin particles was seen (*B*, *arrows*). In the absence of intermediate filaments, wild type (*C*) and R120G αB-crystallin (*D*) both formed discrete 15–20-nm particles (*arrowheads*). *Bar* = 100 μm.

The R120G Mutation Affects the Stability of αB-crystallin at Elevated Temperatures—At elevated temperatures it has been shown that α-crystallin adopts a more disordered structure (53). A conformational transition with a midpoint at 60–62 °C was observed by Fourier-transform infrared spectroscopy, differential scanning calorimetry, and circular dichroism (53). Using the latter method and monitoring the temperature dependence of ellipticity at 205 and 217 nm, a gradual transition was observed for wild type, but not R120G αB-crystallin, over the temperature range of 25–55 °C (see also Fig. 2*A*). Thus, in contrast to α-crystallin (50, 53), consisting of αA- and αB-crystallin subunits, αB-crystallin alone does show a gradual conformational transition in this temperature range. This is not seen for R120G αB-crystallin, as expected from comparing the CD spectra at 25 and 45 °C, which are very similar (Fig. 2*B*). At 64.5 °C and 57.2 °C, however, the heat-induced precipitation of wild type and R120G αB-crystallin, respectively, was 50% complete as measured by light scattering. The different profile of temperature-induced protein aggregation of R120G αB-crystallin compared with wild type αB-crystallin may reflect the increased polydispersity of the mutant protein complexes, but this needs further experimentation.

These data do indicate, however, that αB-crystallin is first stabilized by αA-crystallin, as α-crystallin does not precipitate even at 100 °C (54). Second, these data indicate that the mutation has increased the susceptibility of the protein to temperature-induced unfolding leading to protein precipitation (Fig. 4). Therefore, the mutation decreases protein stability, but the effects are most readily seen at non-physiological temperatures. Nevertheless, the more important question is whether these structural and stability changes caused by the R120G mutation affect the biological activity of αB-crystallin.

Previous studies made a very important correlation between structural changes in α-crystallin proteins and their chaperone activity (12, 50, 55). Using hydrophobic probes, a transition at 30 °C was identified. The exposure of these hydrophobic surfaces was correlated with an increase in the observed chaperone activity of the α-crystallin proteins (12, 50). It has been suggested that the polydisperse quaternary structure of αB-crystallin oligomers (56) is an important feature of the chaperone activity (12). In other studies on αA-crystallin, however, it has been possible to uncouple the changes in secondary and quaternary structure from the chaperone activity (52). Thus, although the R120G mutation causes changes in the protein structure and stability, it is important to assess the effect of the mutation upon the chaperone function of αB-crystallin.

Effect of R120G Mutation upon αB-crystallin Activity—*In vitro* assays (9) have been developed to study the protein chaperone function of αB-crystallin utilizing the ability of αB-crystallin to protect other proteins against either heat- or chemically induced denaturation (*e.g.* Refs. 10 and 11). These proteins do not necessarily represent physiological targets for the chaperone function of αB-crystallin, but they have allowed this key function to be studied *in vitro*. The studies presented here demonstrate that the chaperone function of αB-crystallin is significantly compromised, although not completely abolished toward these non-physiological substrates (Table I). In fact, it appeared that R120G-αB-crystallin was a major part of the insoluble pellet with both alcohol dehydrogenase and citrate synthase as target proteins (data not shown), as also reported for lactalbumin (49), suggesting that binding does not absolutely correlate with chaperone activity.

Although these are important assays, they do not address the most obvious feature of DRM, which is the collapse of the intermediate filament network into characteristic aggregates containing αB-crystallin (3, 4). Several *in vitro* assays were used to investigate the effects of αB-crystallin on intermediate filaments (27, 30, 32). The results presented here show some loss in the ability of R120G αB-crystallin to inhibit intermediate filament assembly (Fig. 6), but the most dramatic changes concerned the interaction of R120G αB-crystallin with assembled intermediate filaments. First, the mutation caused αB-crystallin to bind more avidly to intermediate filaments (Fig. 7). Second, R120G αB-crystallin could no longer prevent gel formation by intermediate filaments (Table II). The increase in binding was visualized (Fig. 8) in the negatively stained samples of the intermediate filament-αB-crystallin complexes formed at 37 °C. In the presence of wild type αB-crystallin, limited binding to the assembled intermediate filaments was observed (Fig. 8*A*). In stark contrast, the R120G αB-crystallin bound avidly to the assembled intermediate filaments and even appeared to induce filament clumping (Fig. 8*B*). Filament lengths were comparable in both samples and so, as expected from the sedimentation assay results (Fig. 8; see also Ref. 57), the differences in the solution viscosity were entirely due to the different αB-crystallins. The data show the mutation in αB-crystallin affects all the different aspects of the interaction with intermediate filaments, but the key aspect would appear to be the change in the activity of αB-crystallin with respect to assembled intermediate filaments. The mutation caused increased binding to intermediate filaments, which appears to actively encourage filament-filament interactions. We propose that this, coupled with the loss of the ability of R120G αB-crystallin to prevent those filament-filament interactions seen in the viscosity assay gels, will lead to intermediate filament aggregation. Our observations are supported by the disease pathology that is typified by intermediate filament aggregation coupled with the association of αB-crystallin (3). It is important to realize that both mutations in αB-crystallin and intermediate filament proteins cause such characteristic pathologies. Our data suggest that a similar change in the association of sHSPs as caused by intermediate filament mutations will explain these disease pathologies.

The R120G mutation in αB-crystallin obviously compromises αB-crystallin function *in vivo*, but the disease phenotypes were not seen at birth, appearing only in early adulthood (3) and affecting only the lenses and muscles of individuals carrying the mutation, while the other tissues that express αB-crystallin had no phenotype. Several factors could explain these observations. First, both wild type and R120G αB-crystallin will be expressed together (3). Second, the R120G mutation apparently does not completely abolish the chaperone activity (Table I). Finally, both the eye lens (58) and muscle express other sHSPs, sometimes in high concentrations (59, 60), which could change the sensitivity of the different tissues. Collectively, these factors might help delay the onset of the disease and select the eye lens and muscles as those tissues to be affected by the R120G mutation in αB-crystallin.

Note Added in Proof—Similar effects on the structure and insulin-chaperone activity of αA-crystallin were observed when the equivalent arginine (Arg^{116}) was mutated to cysteine (61).

REFERENCES

1. Goldfarb, L. G., Park, K. Y., Cervenakova, L., Gorokhova, S., Lee, H. S., Vasconcelos, O., Nagle, J. W., Semino-Mora, C., Sivakumar, K., and Dalakas, M. C. (1998) *Nat. Genet.* **19,** 402–403
2. Munoz-Marmol, A. M., Strasser, G., Isamat, M., Coulombe, P. A., Yang, Y., Roca, X., Vela, E., Mate, J. L., Coll, J., Fernandez-Figueras, M. T., Navas-Palacios, J. J., Ariza, A., and Fuchs, E. (1998) *Proc. Natl. Acad. Sci. U. S. A.* **95,** 11312–11317
3. Vicart, P., Caron, A., Guicheney, P., Li, Z., Prevost, M. C., Faure, A., Chateau, D., Chapon, F., Tome, F., Dupret, J. M., Paulin, D., and Fardeau, M. (1998) *Nat. Genet.* **20,** 92–95
4. Goebel, H. H., and Bornemann, A. (1993) *Virchows Arch. B Cell Pathol. Incl. Mol. Pathol.* **64,** 127–135
5. Iwaki, T., Kume-Iwaki, A., Liem, R. K. H., and Goldman, J. E. (1989) *Cell* **57,** 71–78

6. Magin, T. M., Schroder, R., Leitgeb, S., Wanninger, F., Zatloukal, K., Grund, C., and Melton, D. W. (1998) *J. Cell Biol.* **140,** 1441–1451
7. Lowe, J., McDermott, H., Pike, I., Spendlove, I., Landon, M., and Mayer, R. J. (1992) *J. Pathol.* **166,** 61–68
8. Quinlan, R., and van den IJssel, P. (1999) *Nat. Med.* **5,** 25–26
9. Horwitz, J. (1992) *Proc. Natl. Acad. Sci. U. S. A.* **89,** 10449–10453
10. Jakob, U., Gaestel, M., Engel, K., and Buchner, J. (1993) *J. Biol. Chem.* **268,** 1517–1520
11. Takemoto, L., Emmons, T., and Horwitz, J. (1993) *Biochem. J.* **294,** 435–438
12. Raman, B., Ramakrishna, T., and Rao, C. M. (1995) *FEBS Lett.* **365,** 133–136
13. Muchowski, P. J., and Clark, J. I. (1998) *Proc. Natl. Acad. Sci. U. S. A.* **95,** 1004–1009
14. Blakytny, R., Carver, J. A., Harding, J. J., Kilby, G. W., and Sheil, M. M. (1997) *Biochim. Biophys. Acta* **1343,** 299–315
15. Cherian, M., and Abraham, E. C. (1995) *Biochem. Biophys. Res. Commun.* **208,** 675–679
16. Cherian, M., Smith, J. B., Jiang, X. Y., and Abraham, E. C. (1997) *J. Biol. Chem.* **272,** 29099–29103
17. van Boekel, M. A., Hoogakker, S. E., Harding, J. J., and de Jong, W. W. (1996) *Ophthalmic Res.* **28,** 32–38
18. Smulders, R. L. H., Merck, K. B., Aendekerk, J., Horwitz, J., Takemoto, L., Slingsby, C., Bloemendal, H., and de Jong, W. W. (1995) *Eur. J. Biochem.* **232,** 834–838
19. Smulders, R. H. P. H., Carver, J. A., Lindner, R. A., van Boekel, M. A. M., Bloemendal, H., and de Jong, W. W. (1996) *J. Biol. Chem.* **271,** 29060–29066
20. Horwitz, J., Bova, M., Huang, Q. L., Ding, L., Yaron, O., and Lowman, S. (1998) *Int. J. Biol. Macromol.* **22,** 263–269
21. Berengian, A. R., Parfenova, M., and Mchaourab, H. S. (1999) *J. Biol. Chem.* **274,** 6305–6314
22. Muchowski, P. J., Wu, G. J., Liang, J. J., Adman, E. T., and Clark, J. I. (1999) *J. Mol. Biol.* **289,** 397–411
23. Bennardini, F., Wrzosek, A., and Chiesi, M. (1992) *Circ. Res.* **71,** 288–294
24. Wisniewski, T., and Goldman, J. E. (1998) *Neurochem. Res.* **23,** 385–392
25. Iwaki, T., Iwaki, A., Tateishi, J., and Goldman, J. E. (1994) *J. Cell Biol.* **125,** 1385–1393
26. Kato, K., Shinohara, H., Kurobe, N., Inaguma, Y., Shimizu, K., and Ohshima, K. (1991) *Biochim. Biophys. Acta* **1074,** 201–208
27. Nicholl, I. D., and Quinlan, R. A. (1994) *EMBO J.* **13,** 945–953
28. Carter, J. M., Hutcheson, A. M., and Quinlan, R. A. (1995) *Exp. Eye Res.* **60,** 181–192
29. Quinlan, R. A., Carter, J. M., Sandilands, A., and Prescott, A. R. (1996) *Trends Cell Biol.* **6,** 123–126
30. Djabali, K., deNechaud, B., Landon, F., and Portier, M. M. (1997) *J. Cell Sci.* **110,** 2759–2769
31. Muchowski, P. J., Valdez, M. M., and Clark, J. I. (1999) *Invest. Ophthalmol. Vis. Sci.* **40,** 951–958
32. Perng, M. D., Cairns, L., van den IJssel, P., Prescott, A., Hutcheson, A. M., and Quinlan, R. A. (1999) *J. Cell Sci.* **112,** 2099–2112
33. Ralton, J. E., Lu, X., Hutcheson, A. M., and Quinlan, R. A. (1994) *J. Cell Sci.* **107,** 1935–1948
34. Horwitz, J., Huang, Q. L., Ding, L., and Bova, M. P. (1998) *Methods Enzymol.* **290,** 365–383
35. Muchowski, P. J., Hays, L. G., Yates, J. R., III, and Clark, J. I. (1999) *J. Biol. Chem.* **274,** 30190–30195
36. Liang, J., and Rossi, M. (1989) *Invest. Ophthalmol. Vis. Sci.* **30,** 2065–2068
37. Sun, T. X., Das, B. K., and Liang, J. J. N. (1997) *J. Biol. Chem.* **272,** 6220–6225
38. Mach, H., Middaugh, C. R., and Lewis, R. V. (1992) *Anal. Biochem.* **200,** 74–80
39. Sun, T. X., and Liang, J. J. N. (1998) *J. Biol. Chem.* **273,** 286–290
40. Muchowski, P. J., Bassuk, J. A., Lubsen, N. H., and Clark, J. I. (1997) *J. Biol. Chem.* **272,** 2578–2582
41. MacLean-Fletcher, S., and Pollard, T. D. (1980) *Biochem. Biophys. Res. Commun.* **96,** 18–27
42. Liang, J. N., Andley, U. P., and Chylack, L. J. (1985) *Biochim. Biophys. Acta* **832,** 197–203
43. Quinlan, R. A., Hutcheson, C., and Lane, B. (1995) *Protein Profiles* **2,** 801–952
44. Wistow, G. (1985) *FEBS Lett.* **181,** 1–6
45. de Jong, W. W., Caspers, G. J., and Leunissen, J. A. (1998) *Int. J. Biol. Macromol.* **22,** 151–162
46. Litt, M., Kramer, P., LaMorticella, D. M., Murphey, W., Lovrien, E. W., and Weleber, R. G. (1998) *Hum. Mol. Genet.* **7,** 471–474
47. Kim, K. K., Kim, R., and Kim, S. H. (1998) *Nature* **394,** 595–599
48. van den IJssel, P., Norman, D. G., and Quinlan, R. A. (1999) *Curr. Biol.* **9,** R103–R105
49. Bova, M. P., Yaron, O., Huang, Q., Ding, L., Haley, D. A., Stewart, P. L., and Horwitz, J. (1999) *Proc. Natl. Acad. Sci. U. S. A.* **96,** 6137–6142
50. Raman, B., and Rao, C. M. (1997) *J. Biol. Chem.* **272,** 23559–23564
51. Sun, T. X., Akhtar, N. J., and Liang, J. J. (1998) *FEBS Lett.* **430,** 401–404
52. Berengian, A. R., Bova, M. P., and McHaourab, H. S. (1997) *Biochemistry* **36,** 9951–9957
53. Surewicz, W. K., and Olesen, P. R. (1995) *Biochemistry* **34,** 9655–9660
54. Maiti, M., Kono, M., and Chakrabarti, B. (1988) *FEBS Lett.* **236,** 109–114
55. Rao, P. V., Horwitz, J., and Zigler, J. S., Jr. (1994) *J. Biol. Chem.* **269,** 13266–13272
56. Haley, D. A., Horwitz, J., and Stewart, P. L. (1998) *J. Mol. Biol.* **277,** 27–35
57. Porter, R. M., Hutcheson, A. M., Rugg, E. L., Quinlan, R. A., and Lane, E. B. (1998) *J. Biol. Chem.* **273,** 32265–32272
58. Collier, N. C., and Schlesinger, M. J. (1986) *Exp. Eye Res.* **43,** 103–117
59. de Jong, W. W., Zweers, A., Versteeg, M., and Nuy-Terwindt, E. C. (1984) *Eur. J. Biochem.* **141,** 131–140
60. Inaguma, Y., Goto, S., Shinohara, K., Hasegawa, K., Ohshima, K., and Kato, K. (1993) *J. Biochem.* (*Tokyo*) **114,** 378–384
61. Kumar, L. V. S., Ramakrishna, T., and Rao, C. M. (1999) *J. Biol. Chem.* **274,** 24137–24141

The Cardiomyopathy and Lens Cataract Mutation in αB-crystallin Alters Its Protein Structure, Chaperone Activity, and Interaction with Intermediate Filaments *in Vitro*

Ming Der Perng, Paul J. Muchowski, Paul van den IJssel, Gabrielle J. S. Wu, Aileen M. Hutcheson, John I. Clark and Roy A. Quinlan

J. Biol. Chem. 1999, 274:33235-33243.
doi: 10.1074/jbc.274.47.33235